Engineered Science
DOI: https://dx.doi.org/10.30919/es1257

An Insight into the Electronic and Optical Characteristics of $BaCu_2As_2$ and α-$BaCu_2Sb_2$ Compounds: An *Ab initio* Study

Ali H. Reshak[1, 2, 3,*] and Muhammad M. Ramli[3]

Abstract

This report presents the first principle calculations of the electronic and optical characteristics of $BaCu_2As_2$ and α-$BaCu_2Sb_2$ metallic compounds. The full potential linear augmented plane-wave (FPLAPW) technique is the basis for these computations. The exchange-correlation energy involves the contributions from the local density approximation (LDA), generalized gradient approximation (GGA) and Engel-Vosko generalized gradient approximation (EVGGA). As the EVGGA show better band splitting comparing to LDA and GGA therefore, we show the results of this approximation. The computed electronic band structures illustrate metallic nature of these compounds due to band's overlapping at the Fermi energy. The electronic density of states (total and partial DOS) of these compounds reveals that there exists strong hybridization between As/Sb-*p* and Cu-*d* states, with weak hybridization between Ba-*s* and Cu-*s* states and also between Cu-*d* and As-*d* states below the Fermi level (E_F). The As/Sb-*p* and Ba-*d* states contribute predominantly to the DOS at and above E_F. The origin of different features of optical properties are discussed based on band structure. The α-$BaCu_2Sb_2$ compound demonstrates improved behavior in reflectivity as compared to that of $BaCu_2As_2$ compound. Due to this fact, the ability of reflecting solar light in α-$BaCu_2Sb_2$ compound is more robust than that of $BaCu_2As_2$.

Keywords: Electronic properties; Density of states; Local density approximation; Optical characteristics.
Received: 01 July 2023; Revised: 03 March 2024; Accepted: 04 May 2024.
Article type: Research article.

1. Introduction

The modernization in superconductivity particularly in ternary pnictides and chalcogenides having tetragonal symmetry created prominence in the research area related to the discovery of superconductivity in the related iron-based compounds such as LaFePnO, LiFePn, and $BaFe_2Pn_2$ involving pnictogen (Pn) elements.[1-5] The investigation on these iron-based superconductors was successively expanded into systems including other 3*d* transition metals. The experiments involving chemical doping in an anti-ferromagnetic $BaFe_2As_2$ led to superconductivity by electron incorporation using cobalt (Tc = 22 K)[6] but not using chromium.[7]

Fe chemical substitution with other 3*d* transition metals consequences in a lot of different behaviors that consist of itinerant anti-ferromagnetism in $BaCr_2As_2$,[8] anti-ferromagnetic insulation in $BaMn_2As_2$,[9] correlated metallic effects in $BaCo_2As_2$, and superconductivity in $BaNi_2As_2$ (Tc = 0.6 K).[10] The theoretical study on $BaCu_2As_2$ compound illustrates its metallic and nonmagnetic behavior, with low-lying Cu-*d* states.[11] The option of picking transition metals not only prompts the physical properties, but also influences the chemical bonding in these phases. Transition metals with additional electrons in the 3*d* orbitals acquire the configuration of homo-atomic Pn–Pn bonds that fix two nearby layers, and eventually, deform 2D structure into 3D network.[12] The shaping of Pn_2 dimers is an imperative factor, which not only affects the crystal and electronic structures, magnetism, but also the existence of superconductivity in ternary pnictides with $ThCr_2Si_2$-type structures.[13–16] Previous studies by Pilchowski *et al*.[17] demonstrate that $Ba_2Cu_3P_4$ is four times Cu deficit derivative of $ThCr_2Si_2$-structure, and $BaCu_2As_2$ crystallizes with $ThCr_2Si_2$ structure. While $BaCu_2Sb_2$[18] is based on $ThCr_2Si_2$- and $CaBe_2Ge_2$-type fragments with 1:2 ratio. In addition, some new diluted magnetic semiconductors involving hole- and spin-doped $BaZn_2As_2$ with 122-like phases were investigated by means of the first-principles

[1] *Physics Department, College of Science, University of Basrah, Basrah, 61004, Iraq.*
[2] *Shatt Al-Arab University College, Basra, 61004, Iraq.*
[3] *Center of Excellence Geopolymer and Green Technology (CEGeoGTech), University Malaysia Perlis, Perlis, Kangar 01007, Malaysia.*
**Email:* maalidph@yahoo.co.uk (A. H. Reshak)

calculations for basic structural, elastic, electronic properties and the peculiarities of the inter-atomic bondings.[19] Though the physical properties of phosphide and arsenide compounds are not much recognized, β-$BaCu_2Sb_2$ appears to be a metallic compound with temperature-independent diamagnetic conduct.[20] Saparov *et al.*[21] has reported the synthesis, electrical resistivity, magnetization, single crystalline and powder X-ray diffraction investigations of $BaCu_2As_2$, $BaCu_2Sb_2$, and $Ba_2Cu_3P_4$ compounds. They also studied the thermal transport properties and Seebeck coefficients for $BaCu_2As_2$ resulting in small thermoelectric figure of merit. All of these compounds crystallize in different structures revealing close relation between them.[21]

The present work was planned to study the electronic band structure, density of states, and also the optical properties of $BaCu_2As_2$ and α-$BaCu_2Sb_2$ using the full potential linear augmented plane wave (FP-LAPW) method within the framework of density functional theory (DFT). The computational method is discussed in the following Section 2. While section 3 reveals and explains the computed results and the short conclusion is presented in Section 4.

2. Computational method

The crystal structure of $BaCu_2As_2$ and α-$BaCu_2Sb_2$ has been illustrated in Fig. 1. These compounds possess tetragonal structure with space group D_{4h}^{17} I4/mmm and D_{4h}^{7} P4/nmm for $BaCu_2As_2$ and α-$BaCu_2Sb_2$, respectively.[22] The lattice constants for $BaCu_2As_2$ and α-$BaCu_2Sb_2$ compounds are a = b = 4.4119(4) and 4.6536(3) Å and c = 10.193(2) and 10.7946(13) Å, respectively.[21] The present calculations are performed using the full potential linearized augmented plane-wave (FPLAPW) method based on the DFT[23,24] as implemented in the Wien2k code.[25] The exchange–correlation potentials are determined using the local density approximation (LDA), generalized gradient approximation (GGA) and Engel-Vosko generalized gradient approximation (EVGGA).[26] The Kohn–Sham wave functions are expanded in terms of spherical harmonic functions inside the non-overlapping muffin-tin spheres (MT spheres) surrounding the atomic sites and in the Fourier series at the interstitial region. In the muffin-tin spheres of radius R_{MT}, l-expansion of the non-spherical potentials and charge density was carried out up to $l_{max} = 10$, while the magnitude of the largest vector in charge density Fourier expansion is $G_{max} = 12$ $(Ryd)^{1/2}$. The plane-wave cut-off $K_{max} = 8.0/R_{MT}$ is chosen for the expansion of wave functions at the interstitial site. The Ba, Cu, and As/Sb muffin-tin sphere radii are chosen as 2.0 Bohr. A mesh of 1000 special **k**-points is made in the irreducible wedge of the first Brillouin zone (IBZ).

For analyzing the produced data and matching it with complex optical properties, Kramers-Kronig (KK) equations have been utilized. These equations facilitate to determine the real part of optical parameters by knowing their imaginary counterparts at all frequencies and vice versa. In the present case the imaginary part of the dielectric functions$\varepsilon_2(\omega)$ has been computed using the following equation:[27]

$$\varepsilon_2^{ab}(\omega) = \sum_{nm} \int d\vec{k} f_{nm} \frac{\vartheta_{nm}^{\alpha}(\vec{k})\vartheta_{mn}^{\beta}(\vec{k})}{\omega_{mn}^2} \delta\left(\omega - \omega_{mn}(\vec{k})\right) \quad (1)$$

where ω determines the photon energy and $\omega_{mn}(k)$ gives the energy difference *i.e.*, $\omega_{mn}(k) = E_m(k) - E_n(k)$. The integration is performed over the first IBZ.

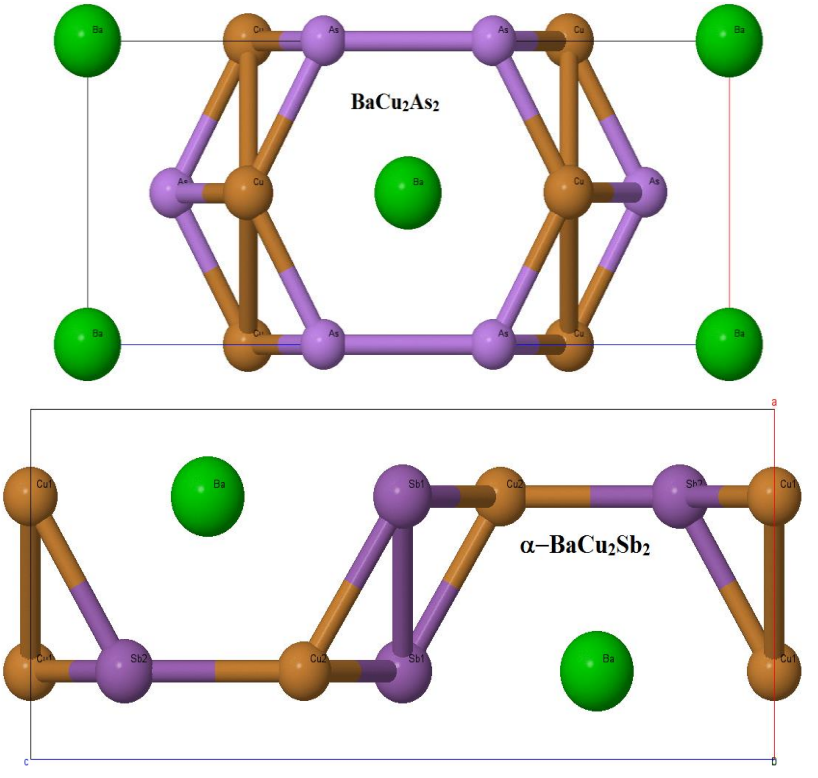

Fig. 1 Unit cell structures of $BaCu_2As_2$ and α-$BaCu_2Sb_2$ compounds.

3. Results and discussion

3.1 Electronic structure

The calculated self-consistent electronic band structures (BS) along the high symmetry directions for $BaCu_2As_2$ and α-$BaCu_2Sb_2$ compounds using EVGGA are demonstrated in Fig. 2. It is a well-known fact that being simple LDA and GGA approaches possess insufficient flexibility to accurately imitate both the exchange–correlation energies as well as their charge derivatives. Keeping in mind such shortcomings, Engel and Vosko developed a new functional form of GGA having capability for the reproduction of better exchange potentials at the expense of less agreement with the exchange energy. Such approach, named EVGGA, reveals relatively better band splitting and some other parameters that are mainly dependent on the exactness of exchange–correlation potentials. That is why, present results are being discussed only on the basis of EVGGA approach.[28]

For the energy band calculations, Fermi level was set to be at 0.0 eV. Fig. 2 demonstrates the formation of impurity/localized states inside the band gap region close to Fermi level showing slight overlap of band states at the Fermi level in the case of $BaCu_2As_2$. However, due to the transfer of density of states from the valence to conduction band region, there exists strong overlapping of states at the Fermi level in the case of α-$BaCu_2Sb_2$ compound. It can be seen that several localized type energy states are distributed between the conduction as well as valence band and Fermi level in the band structure of α-$BaCu_2Sb_2$ compound. Such states may be created due to the contribution of spin-up and spin-down electrons making band structure relatively complex. Because of this, valence band maximum (VBM) extends towards Fermi level and to the conduction band minimum (CBM); consequently, there is no band gap region. This is very much favorable for the enhancement of electrical conductivity of α-$BaCu_2Sb_2$ compound as compared to $BaCu_2As_2$ compound.[29]

Figure 3(a) illustrates the calculated total density of state (TDOS) dispersion of $BaCu_2As_2$ and α-$BaCu_2Sb_2$ compounds using EVGGA approximation. It is noticed that the peaks of α-$BaCu_2Sb_2$ shifts towards higher energies with respect to $BaCu_2As_2$ as shown in Fig. 3(a). The total density of state of both compounds appears to be analogous except a few peaks depict different trend. Moreover, the magnitudes of TDOS peaks for $BaCu_2As_2$ compound are much smaller than those of α-$BaCu_2Sb_2$ compound. It is also obvious from these plots that both the valence and conduction bands overlap at the Fermi level illustrating zero band gap.

DOS plots provide a widespread representation of the elemental contributions to the electronic structure of various substances. DOS was calculated at Fermi level for these two ($BaCu_2As_2$ and α-$BaCu_2Sb_2$) compounds. The metallic character of both compounds is clearly visible from the nonzero DOS at the Fermi level as illustrated by Figs. 3(a-c). Fig. 3(b) clearly demonstrates strong contributions of Ba-*p* and As-*s* states with weak contributions of As-*s* and Cu-*s*/*p* states at about -14.0 eV and -11.0 eV, respectively. In addition, it is clear from Fig. 3(b) that the bands which exist in the energy range from -6.0 to 0.0 eV for $BaCu_2As_2$ compounds are due to Ba-*s* and Cu-*d* states along with weak involvement of the *s* state of Cu and As atoms, and also the *p* state of As and Cu atoms. Particularly a strong peak at about -3.0 eV is predominantly due to the Cu-*d*, and *s* states, As-*d* and Ba-*s* states. Similarly, Fig. 3(c) illustrates strong contributions at -14.0 eV and -9.0 eV caused by Ba-*p*, Sb-*s* states and Cu-*s*/*p* and Sb-*s* states with weak support from other states for the α-

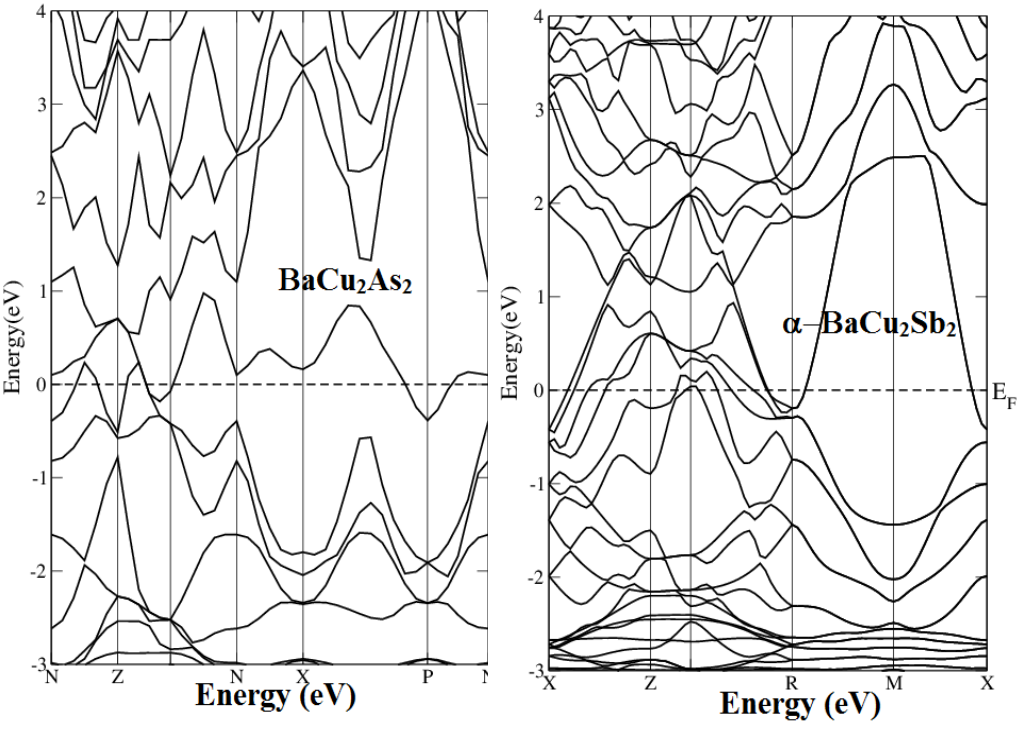

Fig. 2 Calculated band structures of $BaCu_2As_2$ and α-$BaCu_2Sb_2$ compounds.

$BaCu_2Sb_2$ compound. Whilst, in the energy range from -6.0 to 0.0 eV, dominant role is played by Cu-*d* states along with contributions from Sb-*p* and Cu-*s* states. A strong peak at about -3.0 eV is predominantly caused by Cu-*d*, and Sb-*p* states for the α-$BaCu_2Sb_2$ compound. In the vicinity of -3.0 eV band, strong hybridization exists between As/Sb-*p* and Cu-*d* states, with weak hybridization between Ba-*s* and Cu-*s* states and also between Cu-*d* and As-*d* states below the Fermi level. It is also noteworthy that the *p* states of As or Sb and Ba-*d* states mainly take part to add up in the density of states at the Fermi level. The present results are comparable with those of Wu *et al*.[22] The collection of bands that are located above the Fermi level are mainly due to the Ba-*d*, Cu-*s*/*p* states and *p* states of As or Sb, whereas Cu-*s* and Cu-*p* states depict strong hybridization, these states also hybridize with Ba-*d* and As/Sb-*d* states which appears to account for the strong metallic character of these compounds. As most of the Cu-d states are observed at around 3.0 eV below the Fermi energy, the d orbital of Copper appears to be completely filled.[22] Wu *et al*.[22] suggested that the As-As interlayer bonding could not be responsible for Cu-$3d^{10}$ configuration in $BaCu_2As_2$. Certainly, Cu-*d* states in α-$BaCu_2Sb_2$ are observed at almost the same energy as in $BaCu_2As_2$, in spite of the fact that Sb-Sb direct interlayer bonding are absent in the $BaCu_2As_2$ compound.[22] In addition, Cu substitution appears as electron doping signifying that the local As-As and As-transition metal bonding are strongly affected.

Total DOS observed at Fermi level, $N(E_F)$, for $BaCu_2As_2$ and α-$BaCu_2Sb_2$ compounds are obtained as 1.37 and 3.16 states/eV-unit cell as obvious from Fig. 3(a). This figure illustrates that $N(E_F)$ is lower for $BaCu_2As_2$ as compared to that of α-$BaCu_2Sb_2$. The electronic specific heat coefficient (γ) has also been calculated, since it is a function of $N(E_F)$ as expressed by the relation[27,30-37]

$$\gamma = \frac{1}{3}\pi^2 N(E_F){k_B}^2 \quad (2)$$

where k_B represents the Boltzmann constant. The calculated values of γ are equal to 0.237 and 0.548 mJ/mol-K^2 in the case of $BaCu_2As_2$ and α-$BaCu_2Sb_2$, respectively. It is noticeable from Figs. 3(b) and 3(c) that key additions to the occupied region of DOS of valence band arises from the *d* states of Cu atoms and *p* states of Ba atoms, this behavior shows that the 'd' electrons of Cu atom transfer to the Ba sites.

3.2 Optical characteristics

For the justifications of variations and anomalies noticed in the optical spectra, it is normal routine to discuss transformations from occupied to unoccupied bands in the electronic energy band diagram particularly at those points depicting high symmetry in the Brillouin zone.[38] On the basis of electronic configuration, dielectric function given by $\varepsilon(\omega) = \varepsilon_1(\omega) + i\varepsilon_2(\omega)$ of $BaCu_2As_2$ and α-$BaCu_2Sb_2$ compounds was calculated. As these compounds are crystallized in the tetragonal symmetry {having space group D_{4h}^{17} I4/mmm for $BaCu_2As_2$ and D_{4h}^{7} P4/nmm for α-$BaCu_2Sb_2$[22]}. Such symmetry groups depend upon two dominantly independent components of dielectric tensor such as $\varepsilon^{xx}(\omega) = \varepsilon^{yy}(\omega)$ and $\varepsilon^{zz}(\omega)$ associated with the applied electric field resulting from the polarization of light and are found perpendicular as well as parallel to the c-axis. As these two compounds show metallic nature that is why the intraband transitions related to Drude term hasve also been included in the calculations. Hence, the calculations involve the contributions of both the interband and the intraband transitions:

$$\varepsilon_2(\omega) = \varepsilon_{2,inter}(\omega) + \varepsilon_{2,intra}(\omega) \quad (3)$$

The calculated values of both the imaginary $\varepsilon_2(\omega)$ and real $\varepsilon_1(\omega)$ parts of dielectric function in terms of photon energy are presented in Figs. 4(a) and 4(b) respectively. Imaginary part $\varepsilon_2(\omega)$ of the dielectric function has direct relation with the energy band structure.[39] The VBM and the CBM are composed of Ba-*p*, As-*p* and Ba-*d* states respectively. The peaks are located between 0.0 to 5.0 eV for $BaCu_2As_2$ and between 0.0 to 6.0 eV for α-$BaCu_2Sb_2$ compounds corresponding to the transition from As/Sb-*p* VBM to Ba-*d* CBM. The peaks for the calculated components, $\varepsilon_2^{xx}(\omega)$ and$\varepsilon_2^{zz}(\omega)$, for $BaCu_2As_2$ compound lie at different energies however, for α-$BaCu_2Sb_2$ compound, these are located at almost same energy. Such variations of the imaginary component of dielectric function might be related with their slightly different symmetries. In addition, it is noteworthy that all the peaks observed in $\varepsilon_2(\omega)$ are not related with a single interband transformation because a lot of direct to indirect transformations might occur in the band structure with an energy corresponding to the same peaks.[40]

The real part of dielectric function $\varepsilon_1(\omega)$ can be obtained from $\varepsilon_2(\omega)$ using Kramers-Kronig (KK) relation. For real part the calculated components, $\varepsilon_1^{xx}(\omega)$ and $\varepsilon_1^{zz}(\omega)$, show sharp rise below or above 1.0 eV forming maxima at 1.0 or 1.5 eV for $BaCu_2As_2$ and at 2.0 or 2.3 eV for α-$BaCu_2Sb_2$ compounds as demonstrated in Fig. 4. Such a sharp rise might be caused by Drude term representing intraband transitions. There appears a substantial anisotropy noticed between $\varepsilon_1^{xx}(\omega)$ and $\varepsilon_1^{zz}(\omega)$ up to about 7.0 eV, but beyond this energy both components contribute almost equally.

Figure 5 displays the optical functions of $BaCu_2As_2$ and α-$BaCu_2Sb_2$ calculated in the photon energy range of up to 14.0 eV. Figs. 5(a) and 5(b) depict the calculated absorption spectra along xx and zz directions for the $BaCu_2As_2$ and α-$BaCu_2Sb_2$, respectively. These figures reveal that there exists an absorption band in the low energy range below 2.0 eV which might be caused by metallic nature of these compounds. This band shows strong character for the α-$BaCu_2Sb_2$ as compared to that of $BaCu_2As_2$. Moreover, strong anisotropy is noticeable in the absorption spectra of $BaCu_2As_2$ whereas α-$BaCu_2Sb_2$ depicts almost isotropic behavior. As evident from the band structures of these compounds (see Fig. 3) these materials show no band gap, therefore, photoconductivity initiates in both compounds when photon energy is zero, and hence there is a rise in photoconductivity (and consequently the electrical

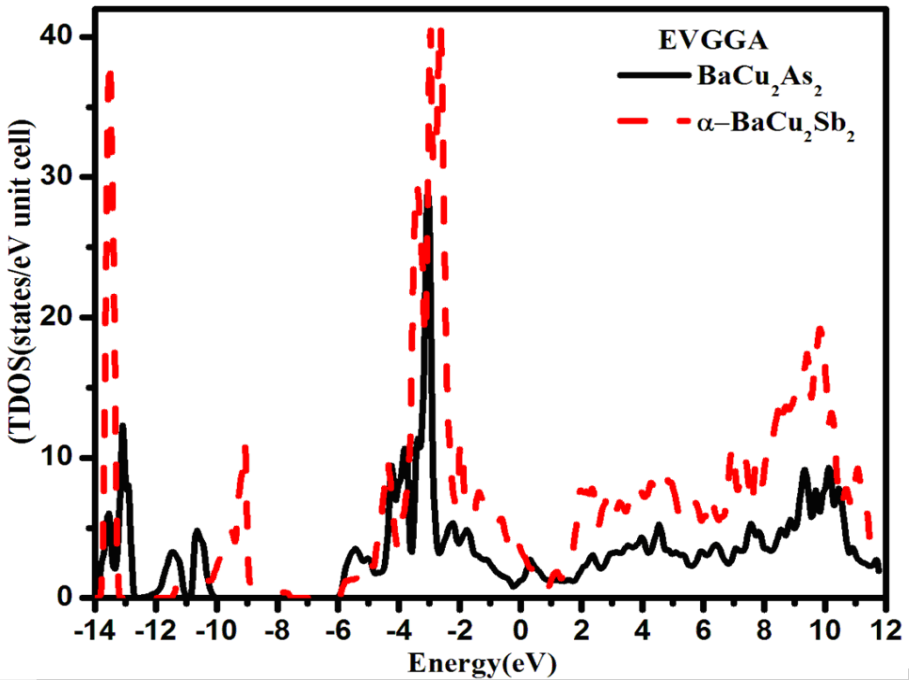
EVGGA
BaCu2As2
α–BaCu2Sb2
(TDOS(states/eV unit cell)
Energy(eV)

(a)

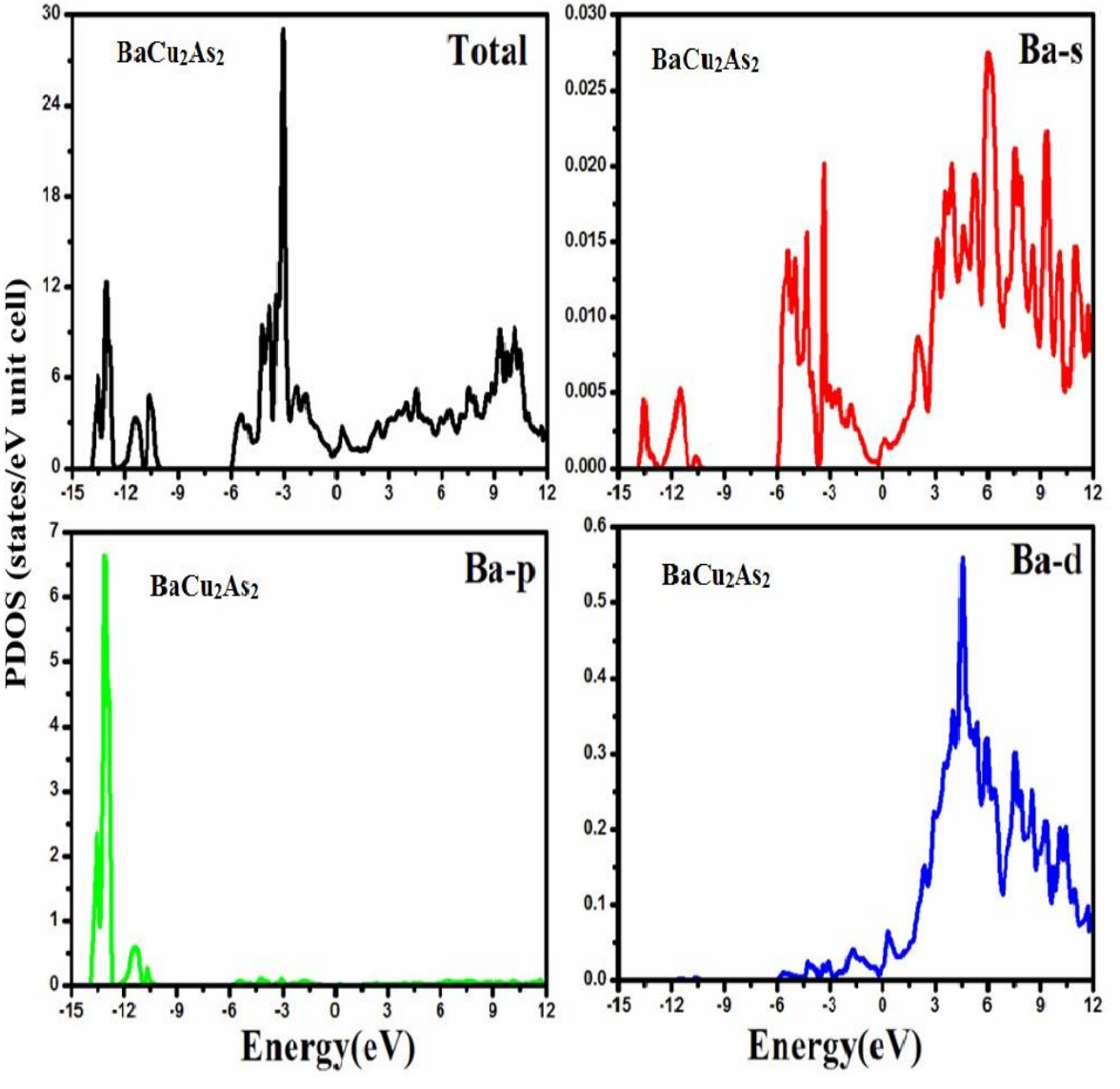
BaCu2As2
Total
Ba-s
Ba-p
Ba-d
PDOS (states/eV unit cell)
Energy(eV)
Energy(eV)

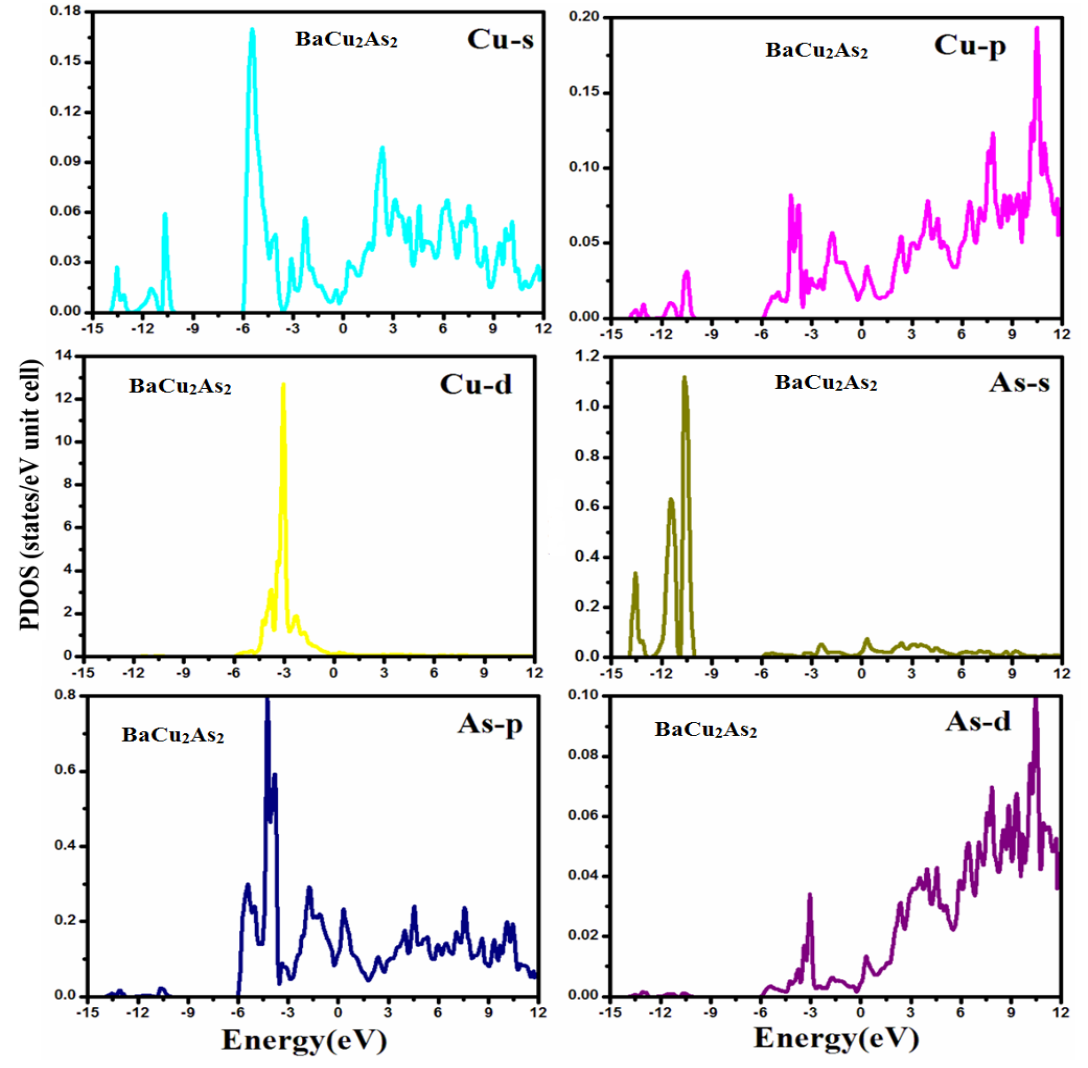

(b)

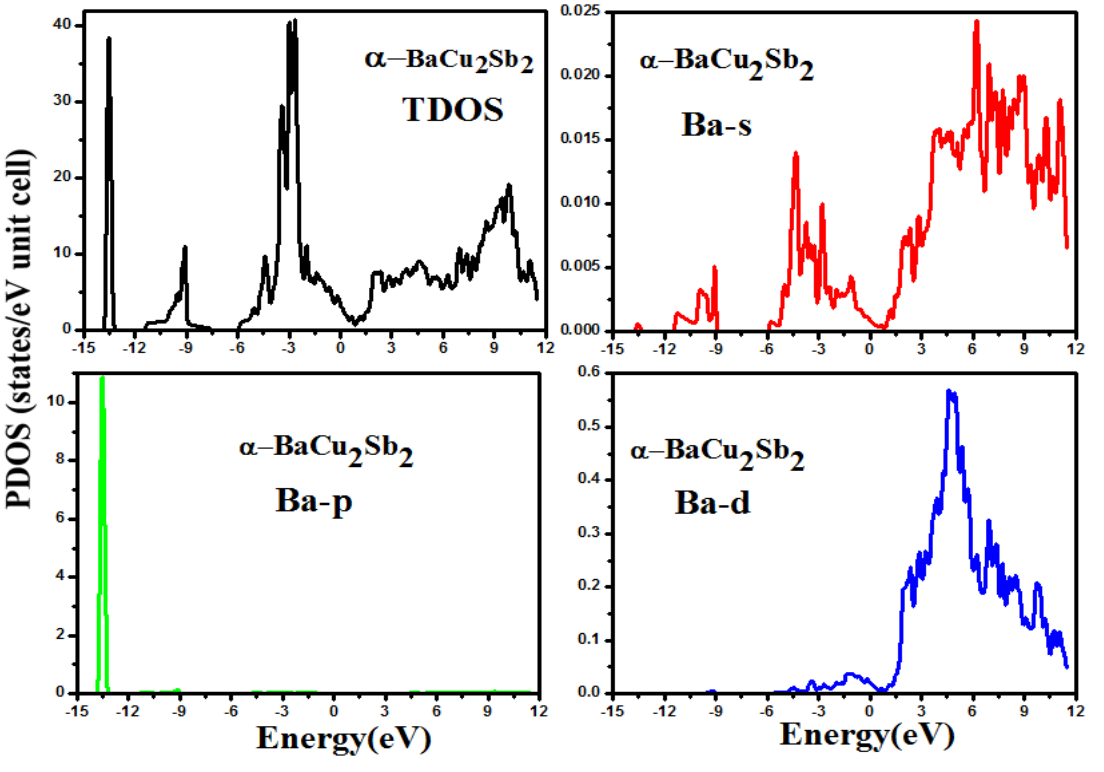

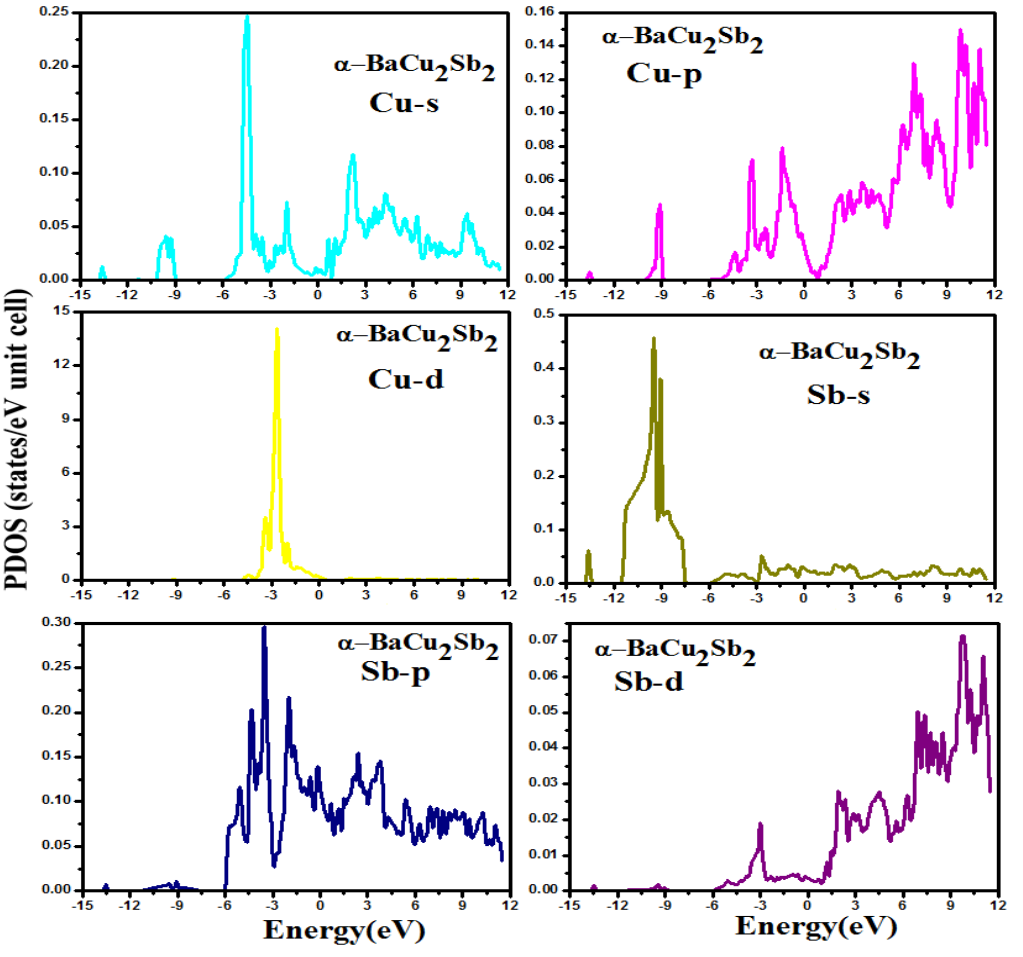

(c)

Fig. 3 Calculated total (a) and partial densities of states (States/eV unit cell) for $BaCu_2As_2$ (b) and for α-$BaCu_2Sb_2$ (c) compounds.

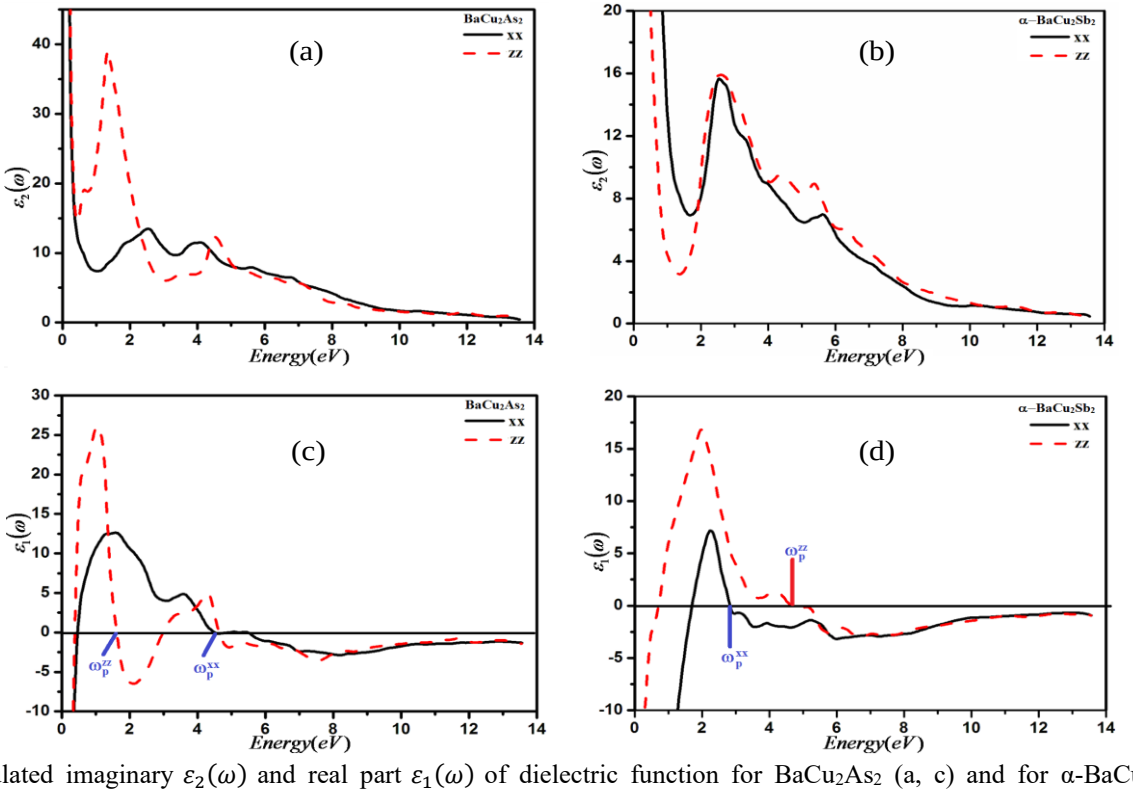

Fig. 4 Calculated imaginary $\varepsilon_2(\omega)$ and real part $\varepsilon_1(\omega)$ of dielectric function for $BaCu_2As_2$ (a, c) and for α-$BaCu_2Sb_2$ (b, d) compounds.

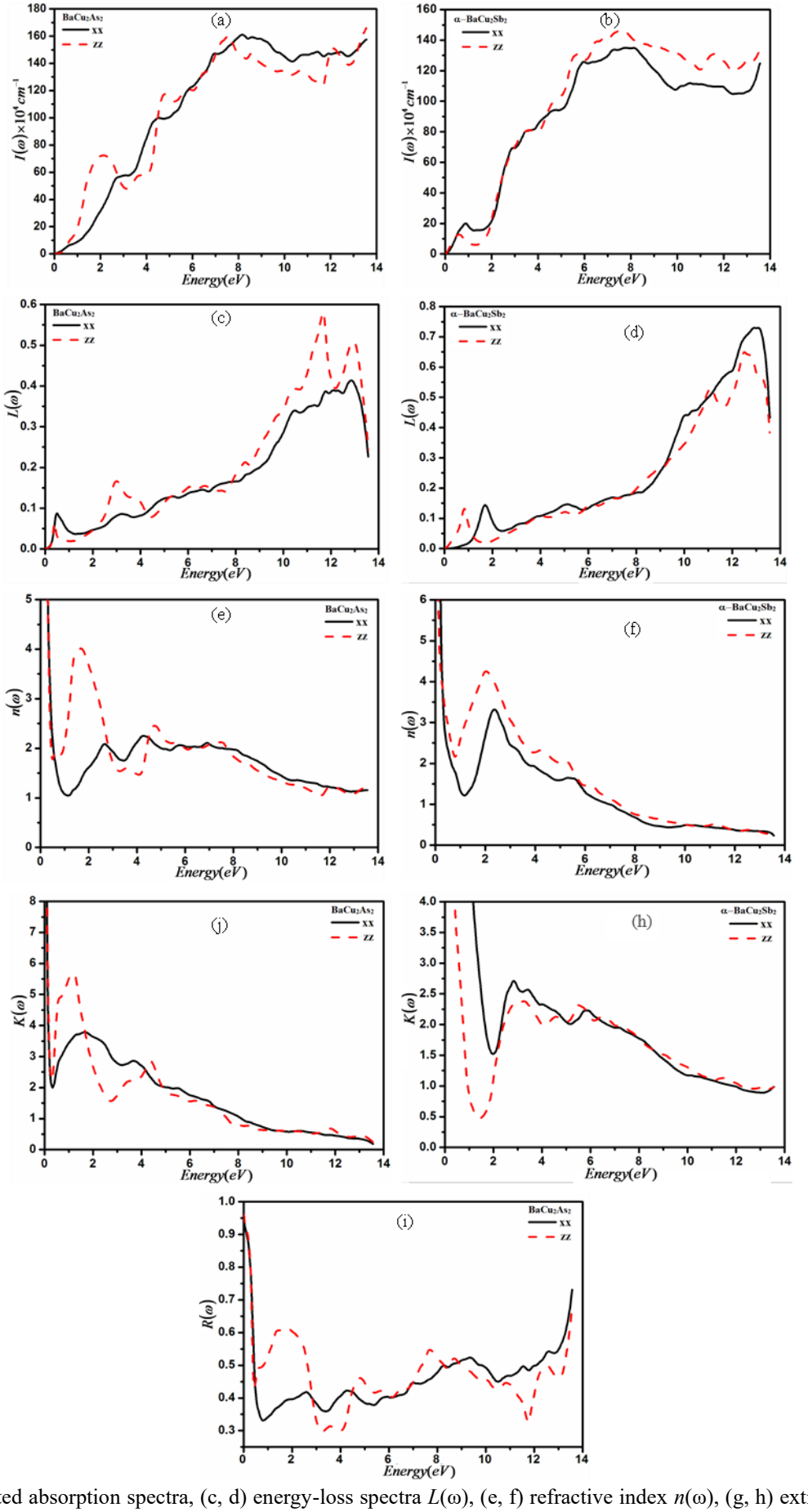

Fig. 5 (a,b) Calculated absorption spectra, (c, d) energy-loss spectra $L(\omega)$, (e, f) refractive index $n(\omega)$, (g, h) extinction co-efficient and (i, j) reflectivity $R(\omega)$ of $BaCu_2As_2$ and α-$BaCu_2Sb_2$ compounds.

conductivity) of these materials by the absorption of photons.

The absorption spectrum of $BaCu_2As_2$ compound raises sharply at a faster rate than that of α-$BaCu_2Sb_2$ compound and illustrates some prominent peaks between 6.0 to 10.0 eV. The first two peaks might be attributed to the transitions from As-*p* to Ba-*d* states. Almost the same features can be seen in the investigated compounds.

The energy-loss spectrum $L(\omega)$ expresses the loss of energy by a fast moving electron traversing in a material.[41] The most intense peak observed in $L(\omega)$ describes the frequency (energy) of combined vibrations of valence electrons inside a crystal and is known as the bulk plasma frequency ω_p, which arises when ε_1 approaches the zero value.[27,42,43] Below ω_p materials illustrate the metallic characteristics (*i.e.* $\varepsilon_1(\omega)<0$).[44] The energy-loss spectrum plot {Figs. 5(c, d)} reveals that the plasma frequencies ω_p are 3.20, 12.85 eV, and 2.94, 11.70 eV of $\omega_p^{xx}(\omega)$ and $\omega_p^{zz}(\omega)$, respectively for $BaCu_2As_2$ while their values for α-$BaCu_2Sb_2$ compounds are 5.10, 12.90 eV, and 5.00, 12.50 eV, respectively as obvious from Figs. 5(c, d). Therefore, as the energy of incident light goes beyond 12.85 eV along xx direction and 11.70 eV along zz orientation, $BaCu_2As_2$ compound becomes transparent. Similarly, for α-$BaCu_2Sb_2$ compound, on raising the frequency of incident light higher than 12.90 eV along xx component and 12.50 eV along zz component, the compound depicts transparent trend. The peaks observed around 12.0 eV are plasma resonances related to the frequency of combined vibrations of valence electrons. However, other peaks might be attributed to excitons and other interband transformations.[27] Since the high-flying climax for $L^{xx}(\omega) = L^{yy}(\omega)$ and $L^{zz}(\omega)$ spectra symbolizes the feature connected with the plasma resonance.[44,45]

The refractive index {having components $n^{xx}(\omega)$ and $n^{zz}(\omega)$} and the extinction coefficient {with components $K^{xx}(\omega)$ and $K^{zz}(\omega)$} related to the complex refractive index have been presented in Figs. 5(e-h). The refractive index $n(\omega)$ also reveals strong anisotropy for the $BaCu_2As_2$ compound however; its trend for α-$BaCu_2Sb_2$ compound is almost identical. For both compounds, the real part, *n* and the imaginary part, k of refractive index demonstrate decreasing trend at high energies as obvious from Figs. 5(e - h).

The calculated reflectivity of $BaCu_2As_2$ and α-$BaCu_2Sb_2$ as a function of photon energy is presented in Figs. 5(i, j). A sudden fall of reflectivity at low energies for both compounds may be associated with their high conductance.[39] It is further noticed that the magnitude of reflectivity for α-$BaCu_2Sb_2$ is somewhat higher than that of $BaCu_2As_2$, which means that the ability of reflecting solar light in α-$BaCu_2Sb_2$ compound is more robust than that of $BaCu_2As_2$.

4. Conclusions

The electronic structure and optical properties have been predicted for the $BaCu_2As_2$ and α-$BaCu_2Sb_2$ compounds. The electronic band structures show the metallic behavior of both compounds. It is observed from the density of states plot that the whole curve of α-$BaCu_2Sb_2$ is shifted towards higher energies about 0.1 eV with respect to $BaCu_2As_2$; and also the peaks of the TDOS for $BaCu_2As_2$ compound are smaller than that of α-$BaCu_2Sb_2$ compound. The band structure helps to discuss the origin of the features that appear in the optical properties. The reflectivity spectrum shows that the predicted compound $BaCu_2As_2$ is a better candidate as compared to those of α-$BaCu_2Sb_2$ compounds as a coating material to avoid solar heating than the improved behavior in reflectivity.

Conflict of Interest

There is no conflict of interest.

Supporting Information

Not applicable.

References

[1] Y. Kamihara, T. Watanabe, M. Hirano, H. Hosono, Iron-based layered superconductor La[$O_{1-x}F_x$]FeAs (x = 0.05–0.12) with T_c = 26 K, *Journal of the American Chemical Society*, 2008, **130**, 3296-3297, doi: 10.1021/ja800073m.

[2] J. Guo, S. Jin, G. Wang, S. Wang, K. Zhu, T. Zhou, M. He, X. Chen, Superconductivity in the iron selenide K$x$$Fe_2Se_2$ ($0 \le x \le 1.0$), *Physical Review B*, 2010, **82**, 180520, doi: 10.1103/PhysRevB.82.180520.

[3] A. S. Sefat, D. J. Singh, Chemistry and electronic structure of iron-based superconductors, *MRS Bulletin*, 2011, **36**, 614-619, doi: 10.1557/mrs.2011.175.

[4] L. Zhang, A. Subedi, D. J. Singh, M. H. Du, Possible superconductivity in Fe-Sb based materials: density functional study of LiFeSb, *Physical Review B*, 2008, **78**, 174520, doi: 10.1103/physrevb.78.174520.

[5] X. C. Wang, Q. Q. Liu, Y. X. Lv, W. B. Gao, L. X. Yang, R. C. Yu, F. Y. Li, C. Q. Jin, The superconductivity at 18 K in LiFeAs system, *Solid State Communications*, 2008, **148**, 538-540, doi: 10.1016/j.ssc.2008.09.057.

[6] A. S. Sefat, R. Y. Jin, M. A. McGuire, B. C. Sales, D. J. Singh, D. Mandrus, *Physical Review Letters*, 2008, **101**, 117004, doi: 10.1103/PhysRevLett.101.117004.

[7] A. S. Sefat, D. J. Singh, L. H. VanBebber, Y. Mozharivskyj, M. A. McGuire, R. Jin, B. C. Sales, V. Keppens, D. Mandrus, Absence of superconductivity in hole-doped $BaFe_{2-x}Cr_xAs_2$ single crystals, *Physical Review B*, 2009, **79**, 224524, doi: 10.1103/physrevb.79.224524.

[8] D. J. Singh, A. S. Sefat, M. A. McGuire, B. C. Sales, D. Mandrus, L. H. VanBebber, V. Keppens, Itinerant antiferromagnetism in $BaCr_2As_2$: experimental characterization and electronic structure calculations, *Physical Review B*, 2009, **79**, 094429, doi: 10.1103/physrevb.79.094429.

[9] Y. Singh, A. Ellern, D. C. Johnston, *Physical Review B*, 2009, **79**, 094519, doi: 10.1103/PhysRevB.79.094519.
[10] A. S. Sefat, D. J. Singh, R. Jin, M. A. McGuire, B. C. Sales, F. Ronning, D. Mandrus, Magnetic, transport, and thermal properties of single crystals of the layered arsenide $BaMn_2As_2$, *Physica C*, 2009, **469**, 350, doi: 10.1016/j.physc.2009.03.025.
[11] D. J. Singh, Electronic structure of $BaCu_2As_2$ and $SrCu_2As_2$: *sp*-band metals, *Physical Review B*, 2009, **79**, 153102, doi: 10.1103/PhysRevB.79.153102.
[12] R. Hoffmann, C. Zheng, Making and breaking bonds in the solid state: the $ThCr_2Si_2$ structure, *The Journal of Physical Chemistry*, 1985, **89**, 4175-4181, doi: 10.1021/j100266a007.
[13] A. I. Coldrea, C. M. J. Andrew, J. G. Analytis, R. D. McDonald, A. F. Bangura, J. H. Chu, I. R. Fisher, A. Carrington, Topological change of the Fermi surface in ternary iron pnictides with reduced c/a ratio: a de Haas-van Alphen study of $CaFe_2P_2$, *Physical Review Letters*, 2009, **103**, 026404, doi: 10.1103/PhysRevLett.103.026404.
[14] S. A. Jia, P. Jiramongkolchai, M. R. Suchomel, B. H. Toby, J. G. Checkelsky, N. P. Ong, R. J. Cava, Ferromagnetic quantum critical point induced by dimer-breaking in $SrCo_2(Ge_{1-x}P_x)_2$, *NaturePhysics*, 2011, **7**, 207, doi: 10.1038/nphys1868.
[15] S. Jia, A. J. Williams, P. W. Stephens, R. J. Cava, Lattice collapse and the magnetic phase diagram of $Sr_{1-x}Ca_xCo_2P_2$, *Physical Review B*, 2009, **80**, 165107, doi: 10.1103/physrevb.80.165107.
[16] K. Kovnir, W. M. Reiff, A. P. Menushenkov, A. A. Yaroslavtsev, R. V. Chernikov, M. Shatruk, "chemical metamagnetism": from antiferromagnetic $PrCo_2P_2$ to ferromagnetic $Pr_{0.8}Eu_{0.2}Co_2P_2$ via chemical compression, *Chemistry of Materials*, 2011, **23**, 3021-3024, doi: 10.1021/cm200782z.
[17] A. Sarkar, A. P. Porter, G. Viswanathan, P. Yox, R. A. Earnest, J. Wang, A. J. Rossini, K. Kovnir, BaCu TP 2 (T= Al, Ga, In): a semiconducting black sheep in the ThCr 2 Si 2 intermetallic family, *Journal of Materials Chemistry A*, 2024, **12**, 10481-10493, doi: 10.1039/D4TA01063A.
[18] J. Dunner, A. Mewis, M. Roepke, G. Michels, New ternary copper pnictides with modified $BaAl_4$ structures, *Zeitschrift Für Anorganische und Allgemeine Chemie*, 1995, **621**, 1523, doi: 10.1002/zaac.19956210915.
[19] I. R. Shein, A. L. Ivanovskii, Elastic, electronic properties and intra-atomic bonding in orthorhombic and tetragonal polymorphs of BaZn2As2 from first-principles calculations, *Journal of Alloys and Compounds*, 2014, **583**, 100-105, doi: 10.1016/j.jallcom.2013.08.118.
[20] V. K. Anand, P. Kanchana Perera, A. Pandey, R. J. Goetsch, A. Kreyssig, D. C. Johnston, Crystal growth and physical properties of SrCu2As2, $SrCu_2Sb2$, and $BaCu_2Sb_2$, *Physical Review B - Condensed Matter and Materials Physics*, 2012, **85**, 214523, doi: 10.1103/PhysRevB.85.214523.
[21] B. Saparov, A. S. Sefat, Metallic properties of Ba_2Cu_3P4 and BaCu2Pn2 (Pn=As, Sb), *Journal of Solid State Chemistry*, 2012, **191**, 213-219, doi: 10.1016/j.jssc.2012.03.036.
[22] S. F. Wu, P. Richard, A. van Roekeghem, S. M. Nie, H. Miao, N. Xu, T. Qian, B. Saparov, Z. Fang, S. Biermann, A. S. Sefat, H. Ding, Direct spectroscopic evidence for completely filled Cu3d shell in $BaCu_2As_2$ and α–$BaCu_2Sb_2$, *Physical Review B*, 2015, **91**, 235109, doi: 10.1103/physrevb.91.235109.
[23] P. Hohenberg, W. Kohn, Inhomogeneous electron gas, *Physical Review*, 1964, **136**, B864-B871, doi: 10.1103/physrev.136.b864.
[24] W. Kohn, L. J. Sham, Self-consistent equations including exchange and correlation effects, *Physical Review*, 1965, **140**, A1133-A1138, doi: 10.1103/physrev.140.a1133.
[25] P. Blaha, K. Schwarz, J. Luitz, WIEN97: A full potential linearized augmented plane wave package for calculating crystal properties, Karlheinz Schwarz, Techn. Universitat Wien, Austria, 1999.
[26] E. Engel, S. H. Vosko, Fourth-order gradient corrections to the exchange-only energy functional: importance of ∇^2ncontributions, *Physical Review B*, 1994, **50**, 10498-10505, doi: 10.1103/physrevb.50.10498.
[27] A. H. Reshak, S. Auluck, I. V. Kityk, Density functional calculations, electronic structure, and optical properties of molybdenum bimetallic nitrides Pt_2Mo_3N and Pd_2Mo_3N, *The Journal of Physical Chemistry B*, 2011, **115**, 3363-3370, doi: 10.1021/jp1116382.
[28] A. H. Reshak, S. Azam, Thermoelectric and optoelectronic properties of a heterocyclic isoxazolone nucleus compound, *Materials Science in Semiconductor Processing*, 2015, **30**, 197-207, doi: 10.1016/j.mssp.2014.10.005.
[29] M. Ullah, A. M. Rana, E. Ahmad, R. Raza, F. Hussain, A. Hussain, M. Iqbal, Phenomenological effets of tantalum incorporation into diamond films: experimental and first principle studies, *Applied Surface Science*, 2016, **380**, 83-90, doi: 10.1016/j.apsusc.2016.02.079.
[30] A. H. Reshak, S. Azam, Thermoelectric, band structure, chemical bonding and dispersion of optical constants of new metal chalcogenides Ba_4CuGa_5Q12 (Q=S, Se), *Journal of Magnetism and Magnetic Materials*, 2014, **362**, 204-215, doi: 10.1016/j.jmmm.2014.02.002.
[31] A. H. Reshak, Y. Al-Douri, R. Khenata, W. Khan, S. A. Khan, S. Azam, Electronic structure, Fermi surface topology

and spectroscopic optical properties of $LaBaCo_2O_{5.5}$ compound, *Journal of Magnetism and Magnetic Materials*, 2014, **363**, 133-139, doi: 10.1016/j.jmmm.2014.03.069.
[32] A. H. Reshak, S. Azam, Density of states, optical and thermoelectric properties of perovskite vanadium fluorides Na_3VF_6, *Journal of Magnetism and Magnetic Materials*, 2014, **358-359**, 16-22, doi: 10.1016/j.jmmm.2014.01.034.
[33] A. H. Reshak, S. Azam, Z. A. Alahmed, J. Chyský, Electronic structure, Fermi surface and optical properties of metallic compound $Be_8(B48)B_2$, *Journal of Magnetism and Magnetic Materials*, 2014, **351**, 98-103, doi: 10.1016/j.jmmm.2013.09.060.
[34] A. H. Reshak, S. Azam, Theoretical study of the structural, electronic structure, Fermi surface, electronic charge density and optical properties of the of LnVO4 (ln= Sm, Eu, Gd and Dy), *International Journal of Electrochemical Science*, 2013, **8**, 10396-10423, doi: 10.1016/s1452-3981(23)13118-x.
[35] A. H. Reshak, S. Azam, First principle study of the electronic structure, Fermi surface, electronic charge density and optical properties of $ThCu_5In$ and $ThCu_5Sn$ single crystals, *Journal of Magnetism and Magnetic Materials*, 2014, **352**, 72-80, doi: 10.1016/j.jmmm.2013.10.009.
[36] S. Azam, A. H. Reshak, Study of electronic structure, charge density, Fermi energy and optical properties of Cs_2KTbCl_6 and Cs_2KEuCl_6, *Physica B: Condensed Matter*, 2013, **431**, 102-108, doi: 10.1016/j.physb.2013.08.048.
[37] S. Azam, S. A. Khan, F. Ali Shah, S. Muhammad, H. U. Din, R. Khenata, Electronic, optical and thermoelectric properties of Ce_3PdIn_{11} and $Ce_5Pd_2In_{19}$: An *ab initio* study, *Intermetallics*, 2014, **55**, 184-194, doi: 10.1016/j.intermet.2014.08.001.
[38] R. D. King-Smith, D. Vanderbilt, Theory of polarization of crystalline solids, *Physical Review B*, 1993, **47**, 1651-1654, doi: 10.1103/physrevb.47.1651.
[39] M. S. Islam, A. K. M. A. Islam, Structural, elastic, electronic and optical properties of a new layered-ternary Ta_4SiC_3 compound, *Physica B: Condensed Matter*, 2011, **406**, 275-279, doi: 10.1016/j.physb.2010.10.067.
[40] B. Xu, L. Yi, First-principle study of the ferroelectricity and optical properties of the $BaBi_2Ta_2O_9$, *Journal of Alloys and Compounds*, 2007, **438**, 25, doi: 10.1016/j.jallcom.2006.08.023.
[41] M. Xu, S. Y. Wang, G. Yin, J. Li, Y. X. Zheng, L.Y. Chen, Y. Jia, Optical properties of cubic Ti_3N_4, Zr_3N_4, and Hf_3N_4, *Applied Physics Letters*, 2006, **89**, 151908-3, doi: 10.1063/1.2360937.
[42] R. Saniz, L.-H. Ye, T. Shishidou, A. J. Freeman, Structural, electronic, and optical properties of $NiAl_3$: first-principles calculations, *Physical Review B*, 2006, **74**, 014209, doi: 10.1103/physrevb.74.014209.
[43] J. S. De-Almeida, R. Ahuja, lectronic and optical properties of RuO_2 and IrO_2, *Physical Review B*, 2006, **73**, 165102-165106, doi: 10.1103/PhysRevB.73.165102.
[44] E. Ece Eyi, S. Cabuk, *Ab initio*study of the structural, electronic and optical properties of $NaTaO_3$, *Philosophical Magazine*, 2010, **90**, 2965-2976, doi: 10.1080/14786431003752159.
[45] A. H. Reshak, K. Nouneh, I. V. Kityk, J. Bila, S. Auluck, H. Kamarudin, Z. Sekkat, Structural, Electronic and Optical Properties in Earth- Abundant Photovoltaic Absorber of $Cu_2ZnSnS4$ and $Cu_2ZnSnSe_4$ from DFT calculations, *International Journal of Electrochemical Science*, 2014, **9**, 955-974, doi: 10.1016/s1452-3981(23)07770-2.